Eur Biophys J (1993) 22:79–95

European Biophysics Journal

Structure of clathrin-coated vesicles from small-angle scattering experiments

Jan Skov Pedersen

Department of Solid State Physics, Risø National Laboratory, DK-4000 Roskilde, Denmark

Received: 10 December 1992 / Accepted in revised form: 22 March 1993

Abstract. Previously published small-angle neutron and X-ray scattering data from coated vesicles, reassembled coats, and stripped vesicles have been analyzed in terms of one common model. The neutron data sets include contrast variation measurements at three different D_2O solvent concentrations. The model used for interpreting the data has spherical symmetry and explicitly takes into account polydispersity, which is described by a Gaussian distribution. A constant thickness of the clathrin coats is assumed. The fitting of the model shows that the coated vesicles consist of a low-density outer protein shell (clathrin) and a central protein shell (accessory polypeptides and receptors) of approximately six times higher density. For the X-ray scattering and neutron contrast variation data, the polydispersity of the samples is of the order of 90 Å (full-width-at-half-maximum value) and the average outer radius is approximately 400 Å. The inner high-density shell has inner and outer radii of 115 and 190 Å, respectively. A simultaneous fit to the three neutron contrast variation data sets identifies the lipid membrane with a thickness of 40 Å and an outer radius of 196 Å. Thus, the membrane and the high-density protein shell overlap in space, which shows that the lipid membrane contains protein. The molecular mass of the average particle is 27×10^6 Da. The coated vesicles consist, on average, of approximately 85% protein and 15% lipids. About 40% of the protein mass is situated in the central high-density shell, which gives a large amount of protein in the lipid membrane. The densities of the central shell and the lipid membrane show that the hydration is small in the central region. A comparison of the total mass, the mass distribution, and the structure of the average-size particles with the barrel structure shows that the accessory polypeptides are incorporated in the lipid membrane. The results from the neutron data for the reassembled coats show that the structure of these particles is very similar to the structure of the native coats. The main difference is a higher density of the central protein shell, which shows that the membrane is replaced by protein in the reassembled coats.

Key words: Clathrin – Coated vesicles – Reassembled coats – Small-angle X-ray and neutron scattering

1. Introduction

The protein clathrin plays an important role in connection with endocytosis in living cells (Pearse and Crowther 1987). The clathrin forms a shell of a polygonal network on the cytoplasmic side of the membrane, stabilizing the structure of the coated vesicle. Clathrin (the heavy chain) is an 180 kDa protein, which forms trimers, termed triskelions (see, e.g. Pearse and Crowther 1987, and references therein). The triskelion is star-shaped molecule of about 800 Å in diameter with kinks at the three legs at about 200 Å from the center of the molecule (Ungewickell and Branton 1981; Crowther and Pearse 1981). Each leg ends in a globular terminal domain. Three light chains of mass ~35 kDa bind to the triskelion, giving a total mass of 630 kDa for the triskelion. (Ungewickell 1983; Kirchhausen et al. 1983). The outer lattice network is formed by packing of the triskelions. The second important component in the coats is the accessory polypeptides (AP). They belong to four classes with masses of approximately 20, 50, 100, and 180 kDa (Unanue et al. 1981; Zaremba and Keen 1983; Pearse and Robinson 1984; Pearse 1985). These polypeptide and complexes of them are believed to form the contact between the clathrin shell and the internal vesicle.

During the formation of the clathrin-coated vesicle, some of the receptor molecules of the cell membrane are incorporated in the membrane of the coated vesicles. These receptor molecules have been observed to have a relatively large extracellular part, with a ligand binding site, and a smaller cytoplasmic part (Perry and Gilbert 1979). In the native coats some receptors have much greater occurrence as compared to the cell membrane, whereas other receptors are nearly completely excluded (Bretscher et al. 1980). Therefore the coats work as

molecular filters, transporting specific molecules into the cell. After the clathrin coats have pinched off from the cell membrane, they disassemble and the clathrin is recycled in the process. Clathrin-coated vesicle and pits are also known to be involved in the process of infection of cells (Marsh and Helenius 1980; Roman and Garoff 1985).

Clathrin coated vesicles can be purified from mammalian cells as first described by Pearse (1975). The constituents of the coated vesicles, clathrin and the accessory polypeptides, can be purified and reassembled into coats without lipid membrane under appropriate conditions (Ungewickell and Branton 1981; Crowther and Pearse 1981; Zaremba and Keen 1983; Pearse and Robinson 1984). In the present work the term *reassembled coats* is used for these, and the term *coated vesicles* is used for the native particles.

Most of the information available on the structure of the coated vesicles and the reassembled coats is from electron microscopy studies. Negative staining has been used for obtaining the structure of the outer clathrin lattice of the coats (Pearse 1975; Crowther et al. 1976; Crowther and Pearse 1981). The clathrin shell is made up of 12 pentagons and a variable number of hexagons. The smallest number of hexagons seems to be four. The internal structure of the coats has been investigated by cryelectron microscopy, in which the coats are incorporated in vitreous ice (Vigers et al. 1986a, b). The micrographs were processed and image reconstructions were performed. For the reassembled coats the 'hexagonal barrel' was selected and investigated. It has a maximum outer size of about 400 Å in radius. The image reconstructions clearly show the outer clathrin shell. They further reveal a central shell between 100 and 200 Å in radius, which is attributed to the accessory polypeptides. Another centered around 250 Å is observed, which is attributed to the terminal domains of the clathrin triskelion. Similar investigations of coated vesicles (Vigers et al. 1986b) are more difficult as the particles are quite polydisperse in size. Studies of individual particles have shown the existence of a shell of high-density situated 250 Å below the outer surface of the coats. This shell was interpreted as being due to proteins possibly incorporated in the lipid membrane. The membrane itself cannot be observed as its electron density is quite similar to that of the surrounding ice.

Deep-etch visualization studies (Heuser and Keen 1988) of coated vesicles have shown that the accessory polypeptides are present as aggregates with a project size of 90×70 Å. The estimated molecular mass of the aggregate is about 300 kDa. The micrographs show that the AP aggregates are often connected to the terminal domains of the triskelions and that enzymatically stripped vesicles have aggregates on the surface. The stripped vesicles have a radius of 200–250 Å in the micrographs.

Coated vesicles and reassembled coats have also been studied by the small-angle scattering technique (Bauer et al. 1991, 1992). The analysis of the data gave a coated vesicle radius of 400–500 Å. A neutron contrast-variation study gave a composition for the coated vesicles of 75% protein and 25% lipids, in agreement with the results of Pearse (1975) obtained by chemical analysis. The molecular mass was determined as 33×10^6 Da. The composition and molecular mass were used for indirectly determining the radius of the membrane. It was found to be 190 Å. However, further analysis was not done as no structural model was available.

The present work concerns a detailed structural analysis of the small-angle scattering data previously published by Bauer et al. (1991, 1992). The data have been analyzed using spherical models consisting of several concentric shells, as is previously described in the literature (Schneider et al. 1978; Chauvin et al. 1978; Sjöberg 1978; Cusack et al. 1985). The model used in the present work is different from these, as it explicitly incorporates polydispersity of the particles. In order to give a clear presentation of the model, a special section has been devoted for describing the details of the model.

The primary advantage of the small-angle scattering technique is that the samples are kept under near-physiological conditions throughout the sample preparation procedure and the measurements. A second advantage concerns the contrast variation technique for neutron scattering, which allows the constituents of the particles to be identified. Furthermore, for neutrons, the scattering contrast of the lipid membrane is quite large for high D_2O solvent concentrations, which means that the technique is quite sensitive to membrane scattering. This sensitivity does not exist for X-ray scattering and electron microscopy. For these techniques the similar electron density of the solvent and lipids leads to a very poor contrast. The aim of the structural analysis is thus to determine the protein distribution in the particles and the position of the lipid membrane. The neutron scattering data, which are on an absolute scale, also give the molecular mass of the particles.

2. Materials and methods

Samples and measurements

As mentioned in the introduction the small-angle scattering data used in the analysis in the present work are the data published by Bauer et al. (1991, 1992). The samples were prepared by G. Jones, M. Behan, and D. Clark in the Biological Support Laboratory at Daresbury Laboratory, UK. The details of the sample preparations are given in Bauer et al. (1991, 1992). The clathrin coated vesicles were purified from bovine brains by successive centrifuging in sucrose gradients and by gel exclusion chromatography. The uncoated vesicles for the X-ray scattering experiments were taken from the low-molecular-weight tail of the elution volume. For the reassembled coats, the coated vesicles were separated into their constituents and the clathrin and accessory polypeptides were purified and reassembled. The details of the experimental procedure for the small-angle X-ray scattering experiments and neutron experiments are described in Bauer et al. (1991, 1992). The data sets are: (*i*) X-ray data on coated vesicles, reassembled coats, and stripped vesicles, (*ii*) neutron contrast variation data on coated vesi-

cles in 0, 42, and 75% D_2O, and (*iii*) neutron data on coated vesicles and reassembled coats in 100% D_2O.

The polydispersity of the samples is of particular interest in connection with finding a model for describing the scattering data. Bauer et al. (1991, 1992) have obtained results for the polydispersity using dynamic light scattering. The measurements were performed on 50–100 times diluted samples in order to get a reasonable signal intensity. For the contrast variation study, the average hydrodynamic radius of the coated vesicles was determined by Bauer et al. (1992) to $R_h = 450 \pm 13$ Å and the average molecular mass was $M = (24 \pm 4) \times 10^6$ Da. The polydispersity factor (the width of a Gaussian size distribution) was determined to $\delta = 30 \pm 5\%$. For the neutron scattering samples in 100% D_2O (Bauer et al. 1991) the light scattering gave $R_h = 470$ Å, $\delta = 35\%$ for the coated vesicles and $R_h = 710$ Å, $\delta = 36\%$ for the reassembled coats. Electron microscopy (Bauer et al. 1991, 1992) qualitatively confirms the presence of relatively large polydispersities. However, the values for the polydispersities are in general smaller.

The relatively large size polydispersity of the coated vesicles deserves comment. The clathrin forms a polygonal network structure around the vesicle, consisting of pentagons and hexagons (Crowther et al. 1976). In order to form a closed coat, 12 pentagons are required, whereas the number of hexagons can be varied. This means that in principle the size of the coat takes on discrete values; however, electron microscopy (Zaremba and Keen 1983; Pearse and Robinson 1984; Ahle and Ungewickell 1986) shows that in practice the distribution of sizes is continuous. Thus in the model presented in the following the distribution is considered to be continuous. The observed polydispersity of 20–30% is much larger that the one determined for samples of influenza virus (Ruigrok et al. 1984a) and of adenovirus (Ruigrok et al. 1984b). For these two virus samples, polydispersities of, respectively, 12 and 6% were found. Compared to the small-angle scattering curves for monodisperse samples, the polydispersity of the clathrin coated vesicles gives rise to a large smearing of the curves. Therefore the polydispersity effects are incorporated explicitly in the models used for analyzing the small-angle scattering results.

Structural models

The data were analyzed using spherical models consisting of several concentric shells as have previously been used in the analysis of small-angle scattering from virus particles (Schneider et al. 1978; Chauvin et al. 1978; Sjöberg 1978; Cusack et al. 1985). The application of models with spherical symmetry means that the finer structural features of the clathrin lattice are neglected. This point is investigated and discussed in the Appendix. The parameters in the models are the radii of the shells R_i and the scattering length density ϱ_i of the shells. These parameters are optimized by means of non-linear least-squares methods. The measured data points are weighted according to their statistical error (Bevington 1969). One of the important differences in the present work, as compared to the previous application of shell models, is that the parameters describing the various smearing effects are not treated as fitting parameters. The variation of the parameters have previously been performed in order to mimic the effects of systematic errors, such as polydispersity effects (Cusack et al. 1985). We have instead included the polydispersity explicitly in the model. However, it is generally recognized that one cannot determine the size distribution *and* the structure of the particle, at the same time, from a scattering curve. This is due to the scattering curve being given as the convolution the size distribution and the form factor. In order to be able to determine the structure it is therefore necessary to assume a particular form the size distribution. In the present work we have chosen a simple form, namely a Gaussian distribution. The shapes of the size distributions determined for reassembled coats (Zaremba and Keen 1983; Pearse and Robinson 1984; Ahle and Ungewickell 1986) are in fact nearly Gaussian.

The cross section for the general model is:

$$\frac{d\sigma(q)}{d\Omega} = \int D(r) F(q,r)^2 \, dr, \tag{1}$$

where $D(r)$ is the Gaussian number size distribution:

$$D(r) = \frac{1}{\sqrt{2\pi\sigma_r^2}} \exp\left(-\frac{r^2}{2\sigma_r^2}\right), \tag{2}$$

and $F(q, r)$ is the form factor of the particle for the deviation r in size relative to the average size.

The variance σ_r of the Gaussian distribution is related to the FWHM value Δr by:

$$\sigma_r = \frac{\Delta r}{2\sqrt{2\ln 2}}. \tag{3}$$

In the rest of the paper Δr is referred to as the polydispersity. Where polydispersities are given in per cent it is Δr relative to the outer radius of the particles. The polydispersities could in principle be fixed at the values determined by other techniques such as, for example, light scattering. However, it was clear from the data analysis that the polydispersity is very sensitive to small changes in the sample preparation procedure. It was therefore taken as a free fitting parameter.

For the X-ray measurements the instrument does not give any significant smearing of the measured scattering curves (Skov Pedersen and Riekel 1991). For the neutron measurements the smearing effects are more pronounced and in the analysis of the neutron data the cross section (1) is convoluted by the instrumental resolution as described by Skov Pedersen et al. (1990). The resolution function $R(\langle q\rangle, q)$ describes the distribution of wave vectors q probed for the nominal vector $\langle q\rangle$. The measured intensity $I(\langle q\rangle)$ is given by:

$$I(\langle q\rangle) = \int R(\langle q\rangle, q) \frac{d\sigma(q)}{d\Omega} \, dq. \tag{4}$$

The analysis by Vigers et al. (1986b) of reassembled clathrin coats and intact coated vesicles by cryo-electron microscopy indicates that the thickness of the clathrin

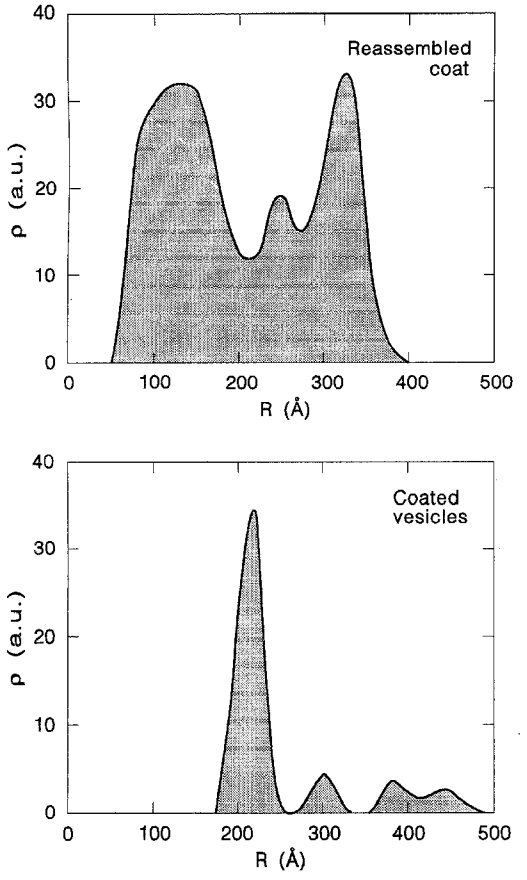

Fig. 1. The radial density distribution for reassembled coats and an intact coated vesicle as derived from the radial mass distributions determined by Vigers et al. (1986 a, b) from cryo-electron microscopy

coat is constant, i.e., independent of particle radius. For the reassembled coats and for some of the coated vesicles, Vigers et al. (1986 b) determined a radial mass distribution. Fig. 1 shows this distribution converted to a radial density distribution for the reassembled coats and for a coated vesicle of radius 475 Å. For the latter, the negative values arising from the phase-contrast ripples have been suppressed. However, some of the oscillations seen in the figure are likely to be due to the these ripples. The density in Fig. 1 is due to the protein in the coats as the lipids have an electron density which is close to that of the water.

The simplest model that can be derived from the density shown in Fig. 1 is a model with two successive shells for the protein and with an empty core:

$$F_p(q,r) = \varrho_1 \Phi(q, R_1 + r) - (\varrho_1 - \varrho_2)\, \Phi(q, R_2 + r) - \varrho_2 \Phi(q, R_3 + r), \quad (5)$$

where R_1 and R_2 are the outer and inner radius of the outer shell and R_3 are the inner radius of the inner shell. The scattering densities of these two shells are ϱ_1 and ϱ_2, respectively. In the equation, $\Phi(q, R)$ is the form factor of a sphere of radius R:

$$\Phi(q,R) = \frac{4}{3}\pi R^3 \frac{3[\sin(qR) - qR\cos(qR)]}{(qR)^3}. \quad (6)$$

For the lipid membrane the form factor was chosen as:

$$F_m(q,r) = \varrho_m[\Phi(q, R_m + r) - \Phi(q, R_m - W_m + r)], \quad (7)$$

where W_m is the width of the membrane. The fits are not very sensitive to the particular value of this parameter, as it has a value (~ 40 Å) which is quite close to the resolution of the data: $\pi/0.1\,\text{Å} = 31$ Å. It was therefore kept fixed at 40 Å in all the fits. This value was estimated from the membrane thicknesses found by Harrison et al. (1971); Schneider et al. (1978); and Cusack et al. (1985).

The total form factor of the model is the sum of the protein and the lipid contributions:

$$F(q,r) = F_p(q,r) + F_m(q,r). \quad (8)$$

For the neutron scattering, the scattering length density ϱ_i of the ith component depends linearly on the D_2O fraction x of the buffer:

$$\varrho_i = \varrho_i^0 (x - x_i^0), \quad (9)$$

where x_i^0 is the match point of the ith component and $\varrho_i^0\, x_i^0$ is the scattering density in pure H_2O. This dependence is used explicitly when fitting the three data sets at different contrasts simultaneously. This approach is in line with the approach first used by Cusack et al. (1985) in the analysis of the scattering data from influenza virus. In all the fits a constant background was also added to the model given in (1) in order to fit residual background in the data.

One of the major problems when fitting the spherical models to the data is a significant correlation between the scattering length densities ϱ_i and the radii of the shells R_i. For the X-ray scattering data, the smearing of the scattering curves is almost entirely due to polydispersity and it appears that the gradients in the different parameters are sufficiently independent to allow a simultaneous fit of the scattering densities, the radii, and the polydispersity. The search procedure of Marquardt (1963) (described also by Bevington 1969) was applied for least-squares method. However, for the neutron scattering data the additional smearing due to instrumental resolution apparently introduces correlations between the parameters, and it is in some cases not possible to fit the parameters simultaneously. In such cases a grid search was applied, in which the parameters are optimized successively and repeatedly (see Bevington 1969). This procedure is time consuming but it converges reliably. Once the minimum is found, the errors were determined from the usual error matrix (Bevington 1969) by fitting all the parameters in the model simultaneously. In some of the fits, the correlation between the parameters remains large even at the minimum and the errors of the correlated parameters are not reliable.

3. Results

Lower resolution model for the X-ray scattering data

The small-angle X-ray scattering was performed by Bauer et al. (1991 on three different samples: Reassembled coats, native coated vesicles, and stripped vesicles. The mea-

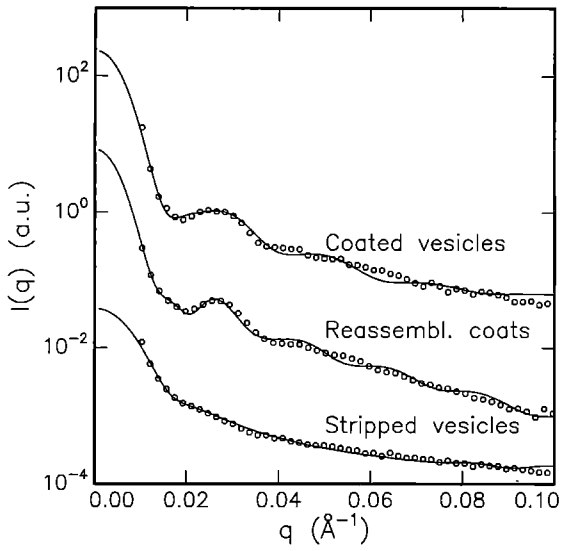

Fig. 2. Small-angle X-ray scattering data. Upper data points: native coated vesicles. Middle data points: reassembled coats. Lower data points: the stripped vesicles. The curves are the fit of the two-shell model for the coated vesicles and the reassembled coats. The curve for the stripped vesicles is the fit of a one-shell model. The statistical errors on the measured data are smaller or equal to the size of the symbols

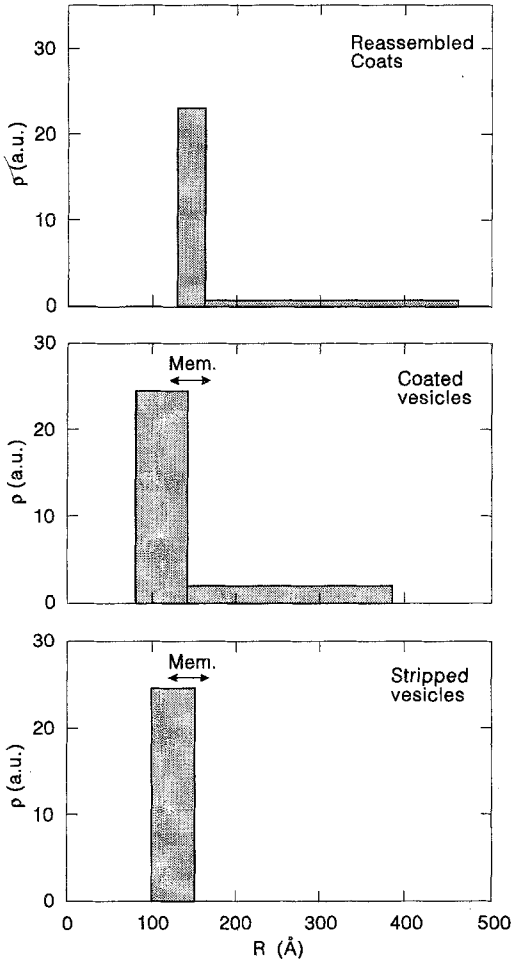

Fig. 3. Average particle radial electron densities, from the X-ray scattering data, of the average particle for the two-shell model for the reassembled coats and the coated vesicles, and the one-shell model for the stripped vesicles. The densities correspond to the fits shown in Fig. 2

Table 1. Results from the X-ray data for the two-shell model for the reassembled coats and the coated vesicles, and the one-shell model for the stripped vesicles. The radii are for the average particle. The densities are in arbitrary units and can only be compared within each column

	Reass. coats	Coated vesic.	Stripped vesic.
Δr [Å]	65±3	93±5	130±6.2
R_1 [Å]	461±4	384±5	–
R_2 [Å]	159±7	137±5	144±5
R_3 [Å]	129±7	79±4	99±6
R_1-R_2 [Å]	302±8	247±6	–
R_2-R_3 [Å]	30±10	58±6	45±8
ϱ_1 [a.u.]	1.6±0.1	2.2±0.1	–
ϱ_2 [a.u.]	46±20	25±1.3	31±4
V_1 [10^8 Å^3]	3.9±0.1	2.3±0.1	–
V_2 [10^6 Å^3]	7.9±2.6	8.7±1.2	8.4±1.5
$M_2/(M_1+M_2)$	0.37±0.05	0.30±0.05	–

sured data are shown in Fig. 2. For the reassembled coats and the coated vesicles a secondary maximum is present around $q = 0.026$ Å^{-1}. The maximum is broadest for the coated vesicles. For the stripped vesicles, the secondary maximum is only weakly present at a slightly smaller scattering vector $q = 0.023$ Å^{-1}.

For X-ray scattering, the contrast is given by the difference in the electron density in the particles and the solvent. For the protein the typical value is 0.08 elect./Å^3, whereas for lipids it is in the range from −0.03 to 0.001, depending on the density of the lipid molecules (Perkins 1988). Thus, the contribution to the scattering from the lipid membrane is much smaller than the contribution from the protein. In the first model we will therefore neglect the scattering from the membrane and take the particle form factor to be equal to the protein form factor (5) consisting of two shells. For the stripped vesicles only one shell is used. The two models have, respectively, 7 and 5 parameters, each including a parameter to describe residual background in the data. The fits of these models to the data are shown in Fig. 2. The models agree quite well with the measured data for $q < 0.04$ Å^{-1}, corresponding to a resolution of about 80 Å.

The parameters resulting from the fits are given in Table 1 and the radial protein densities of the average particles are displayed in Fig. 3. The average outer radius is somewhat larger for the reassembled coats than for the coated vesicles. Both types of particles have a shell of high density of thickness 30–60 Å at a relatively small radius. This shell of high density is also present in the stripped vesicles. The volume of the shell is similar for all three types of particles: $\sim 8 \times 10^8$ Å^3. The polydispersity relative to the average outer particle radius is 14% for the reassembled coats and 24% for the coated vesicles. For the stripped vesicles the absolute value of the polydispersity is significantly larger than for the two other types of particles, probably due to the way this sample was prepared.

The density in the high-density inner shell is about 30 times larger than the density in the outer shell for the reassembled coats. For the coated vesicles, the ratio of the two densities is about 11. Neglecting the possible influ-

ence of the membrane on the form factors, the mass of the protein in the two shells is proportional to the volume times the density of the shell. Using this one can calculate the ratio of the masses in the two shells. For the reassembled coats $37 \pm 5\%$ of the protein mass is in the central shell, whereas for the coated vesicles the central shell contains $30 \pm 5\%$ of the protein mass. The errors on these parameters are estimates and not calculated by the usual error analysis. The scattering densities and the volume of the shells are very correlated, as it is the product of these two entities which is proportional to the scattering amplitude. The correlation of the parameters gives relatively large errors in both parameters. However, the mass, which is proportional to the product of the scattering density and the volume, is a better defined parameter as the scattering amplitude of each component is proportional to the mass.

Contrast variation neutron scattering data

The neutron scattering data recorded by Bauer et al. (1992) for the three contrasts of 0, 42, and 75% D_2O are displayed in Fig. 4. A secondary maximum is clearly present at $q = 0.027$ Å^{-1} in the 0% data, and a weaker maximum is observed in the 75% data. For the 42% data, the scattering length density of the protein is matched, and the secondary maximum is nearly absent.

The analysis we have performed consists of two steps: First, the two data sets in 0 and in 75% D_2O were fitted individually with the model presented in the previous section. Second, all three contrasts were fitted simultaneously, taking into account the known variation (9) of the scattering length density with D_2O concentration. The first step is required in order to have good estimates for the starting parameters in the simultaneous fitting.

The data have previously been analyzed (Bauer et al. 1992) in terms of model-independent information. By assuming monodispersity of the samples a composition of $25 \pm 5\%$ lipids and $75 \pm 5\%$ proteins was found. From the scattering length densities of lipids and protein and their variation with D_2O concentration (Jacrot 1976; Cusack et al. 1985), one finds that the lipids contribute only 12% of the total scattering amplitude at 0% D_2O. At 75% D_2O, the lipids and protein both contribute about 50% of the scattering. Owing to these considerations, we have used the following procedure: First the 0% D_2O data were fitted by including only two shells in the structure factor, that is, we neglected the smaller contribution to the scattering from the lipids. Then the 75% D_2O data were fitted, including a shell to describe the membrane. The scattering length densities in the two shells, also used for the 0% data, were multiplied with a factor of 0.76 in order to take into account the reduction in effective scattering density between 0 and 75%, as expected for protein. Only the parameters describing the membrane were optimized in the second fit.

The fit to the 0% D_2O data is excellent and given parameters that agree very with those found when fitting the X-ray scattering data for the coated vesicles, except for small differences for the high density shell in the center. It has an outer radius of 194 Å and a thickness of 76 Å. The polydispersity is $\Delta r = 70$ Å and the outer radius of the average particle is $R_1 = 391$ Å, giving a relative polydispersity of 18%. When fitting the 75% data, the polydispersity was fixed at the value found for the 0% data. The fit to the data is not quite as good as for the 0% data. The main discrepancies are at low q values where the model intensities are lower than the data. Including the polydispersity into the fits only gave an increase to $\Delta r = 84$ Å with only a minor improvement of the fit. Therefore, the deviations at low q are probably due either to some weak aggregation in the sample or to the presence of a small fraction of larger particles in the 75% data. The fit was very good at large q values, where the model reproduces the weaker secondary maximum in the data. The outer radius of the membrane is 195 Å, which shows that the membrane and the inner high density protein shell overlap.

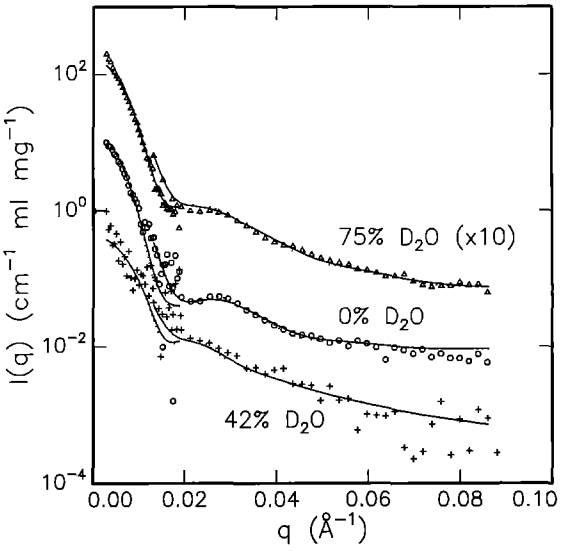

Fig. 4. Small-angle neutron scattering data for coated vesicles. The data are on absolute scale and they are normalized with respect to concentration by dividing with the concentrations in the units mg/ml. The lower, middle, and upper data sets are for 42, 0, and 75% D_2O, respectively. The data for 75% are multiplied by 10. The solid lines are the simultaneous fit of the two-shell model, smeared by instrumental resolution. The dotted lines are the corresponding ideal fit. The statistical errors on the measured data are omitted for clarity but they can be found in Bauer et al. (1992)

In the simultaneous fit to all three data sets, the match points were taken as $x_l^0 = 0.12$ for the lipids and $x_p^0 = 0.42$ for the protein (Jacrot 1976; Cusack et al. 1985). These values were fixed in the fits, so that the prefactors in the linear expression of the scattering length density (9) directly relate to the amount of lipids and protein. The whole range of the measured scattering curves were fitted, and a common size distribution and polydispersity were assumed. The model has nine fitting parameters, including two parameters describing the residual background in the 0 and 75% D_2O data. The 5% uncertainty in the concentrations used for normalization of the data was incorporated in the errors of the experimental data.

The result from the fit for the structural parameters are given in Table 2, and the resulting average density profile

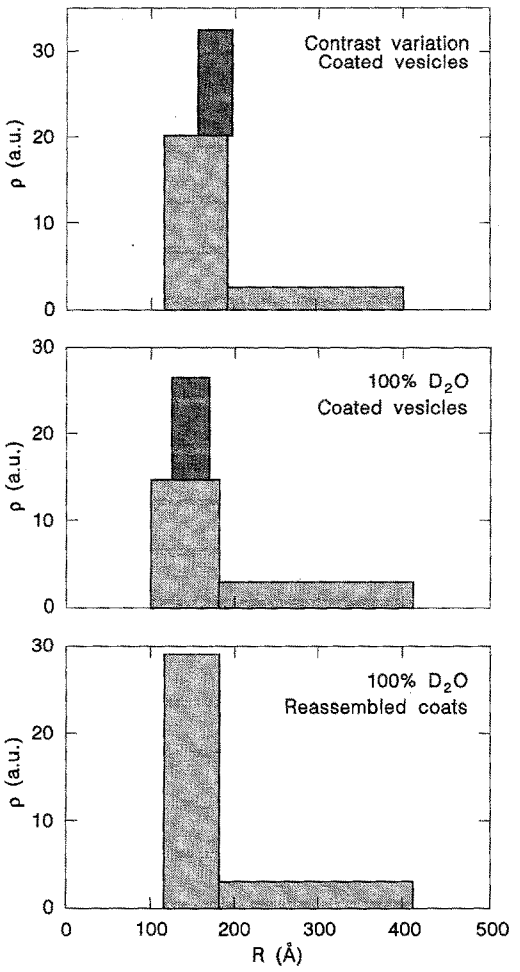

Fig. 5. Average particle radial density profiles from the neutron scattering data. The upper profile is for the coated vesicles from the simultaneous fit of the contrast variation neutron data. The membrane component is dark shaded. The middle part is from the fit to the 100% D_2O data for the coated vesicles. The lower part is from the fit to the 100% D_2O data for the reassembled coats

is shown in Fig. 5. The continuous curves in Fig. 4 are the fits of the model, smeared by instrumental resolution, and the dotted curves are the ideal fits. The fit to the data is very good, and the variation in the shape of the secondary maxima is well reproduced by the model. The polydispersity is 23%, corresponding to the variance $\sigma_r = 38$ Å. Note that the size distribution contains 68% of the particles between $+\sigma_r$ and $-\sigma_r$. In the following analysis we will consider the average particle with radius R_1 as well as those with radius $R_1-\sigma_r$ and $R_1+\sigma_r$. Some results for these three particle sizes are also given in Table 2. The scattering intensity at $q=0$ is weighted approximately as the radius to the power six. The fits are therefore much more sensitive to the large-radius part of the size distribution compared to the small-radius part. The average particle has an outer radius of ~ 400 Å. The coat thickness, defined as the distance from the outer surface of the coat to the outer surface of the membrane, is 200 Å. The central high-density protein shell has a width of 75 Å.

As the size distribution is determined by the fit, various parameters for equivalent monodisperse samples can be calculated. For instance, the forward scattering intensity

Table 2. Results for the neutron scattering data from the simultaneous fit to the three contrast. The results are given for the particles of average size R_1 and those of size $R_1-\sigma_r$ and $R_1+\sigma_r$. M is the total molecular mass, M_p and M_l are the molecular mass of the protein and lipids, respectively, and $M_{p,1}$ and $M_{p,2}$ are the mass of the protein in the outer and inner shell respectively. The polydispersity is: $\Delta r = 90 \pm 5$ Å

	$'R_1-\sigma_r'$	$'R_1'$	$'R_1+\sigma_r'$
R_1 [Å]	359	397±2.6	435
R_2 [Å]	151	190±0.7	228
R_3 [Å]	77	115±1.3	153
R_m [Å]	158	196±0.8	235
M [10^6 Da]	18.7	27.3	37.8
M_p [10^6 Da]	16.3	23.4	32.1
$M_{p,1}$ [10^6 Da]	11.2	14.6	18.4
$M_{p,2}$ [10^6 Da]	5.1	8.9	13.7
$M_{p,2}/M_p$	0.31	0.38	0.43
M_l [10^6 Da]	2.4	3.9	5.7

$I(q=0)$ are 9.4, 14.3, and 20.4 ml/(mg cm) for respectively, the $R_1-\sigma_r$, R_1, and $R_1+\sigma_r$ particles at 75% D_2O. The corresponding overall match points for the three different sizes are respectively, 36.4, 35.9, and 35.5% D_2O. The variation of these parameters with particle size is due to a small variation in the composition. The composition of the particles can be calculated from the match points by using the known values for the scattering length densities (Cusack et al. 1985; Bauer et al. 1992). For the lipids we have $\varrho_l = 10.9\times10^{-14}(x-0.12)$ cm/Da and for protein $\varrho_p = 7.0\times10^{-14}(x-0.42)$ cm/Da. From the match point of the particle the mass fraction M_p/M of the protein can be calculated:

$$M_p/M = \left[1 - \frac{\varrho_p^0(x_0 - x_p^0)}{\varrho_l^0(x_0 - x_l^0)}\right]^{-1}, \tag{10}$$

where x_0 is the match point for the particle and the values of the rest of the parameters are easily found by comparing to the expression for ϱ_p and ϱ_l given above. Using this we find a protein mass fraction of 86% for the average particle, and 87% and 85% for particles deviating $-\sigma_r$ and $+\sigma_r$ in radius, respectively. The statistical errors on these values are quite small ($<\pm1\%$).

Table 2 contains results for the radii of the shells in the model, the total molecular mass, and the molecular mass of the different components, for the average particle as well as those deviating $-\sigma_r$ and $+\sigma_r$ in radius. The total molecular mass is given by:

$$M = \frac{I(0)}{c}\frac{10^3}{N_A \Delta\varrho^2}, \tag{11}$$

where $I(0)/c$ is the observed forward scattering, normalized to the concentration in units mg/ml, N_A is Avogadro's number, and the factor 10^3 converts mg to grams. The scattering contrast $\Delta\varrho$ is given by the composition:

$$\Delta\varrho = \frac{M_p}{M}\varrho_p^0(x - x_p^0) + \left[1 - \frac{M_p}{M}\right]\varrho_l^0(x - x_l^0). \tag{12}$$

The molecular mass of the average particle is $27.3\pm 4\times10^6$ Da. The error is mainly given by the uncertainty

from the determining the absolute scale of the data. Note that the molecular mass of the particle, given in Table 2, varies by a factor of two between the particle of radius $R_1-\sigma_r$ and of radius $R_1+\sigma_r$. For the average particle, 38% of the protein mass is in the central high-density shell.

Neutron scattering data in 100% D_2O

The neutron scattering data recorded by Bauer et al. (1991) for coated vesicles and reassembled coats are shown in Fig. 6. The data for the two types of particles are quite similar, and also similar to the data for 75% D_2O from the contrast variation series. The model from the previous section was fitted to the data. For the coated vesicles the model has 9 parameters and for the reassembled coats it has 7. The fits, smeared by instrumental resolutions are shown in Fig. 6 as full lines, and the ideal curves are shown as dotted lines. The agreement with the measured data is very good except at very low q and close to 0.045 $Å^{-1}$, where small deviations are present.

The radial distribution functions, resulting from the fits, are shown in Fig. 5 and the parameters are displayed in Table 3. When comparing with the results for the contrast variation series one sees that the distributions are very similar with a slightly smaller radius of the membrane for the 100% D_2O data. The coat thickness (the distance from the outer coat surface to the outer membrane surface) is 250 Å. The polydispersities are much larger than for the data sets described above, namely, 42% for the coated vesicles and 38% for the reassembled coats. For comparison, the 75% D_2O data set from the contrast variation series, was also fitted with the model. For this data set, a larger polydispersity can also be expected because the simultaneous fit, described in the previous section, had some deviations at small q. However, the determined polydispersity was only 27%. The larger polydispersity for the 100% D_2O data gives a pronounced smearing of the scattering curve, which causes some loss of information. This might give rise to errors in the density distributions.

The molecular mass of the average-size particle is $36\pm5\times10^6$ Da for the coated vesicles and $26\pm5\times10^6$ Da for the reassembled coats. For the coated vesicles, one can identify the 40 Å thick shell with the lipid membrane, and this gives a composition of 89% protein and 11% lipids of the particles. These numbers have quite large uncertainties, as the identification is based on the assumption that the 40 Å thick shell consists of lipids. The central high-density shell contains 28% of the total protein mass for the coated vesicles and 42% for the reassembled coats.

Higher resolution model for the X-ray scattering data

The fits of the lower resolution model to the X-ray data were not satisfactory at large q, which suggests that additional features (shells) should be included. In this section the best fits of models of higher resolution to the X-ray scattering data are presented. The number of shells in the model was increased until the quality of the fits did not improve. It has not been the intention to use the same model for the three data sets, but rather to find the ones that fit the data best, in order to find possible differences between the three types of particle: Reassembled coats, coated vesicles, and stripped vesicles. However, we note that when introducing more parameters and features in the models, there is a greater risk that a possibly wrong form for the size distribution will give rise to structural features in the individual coats (form factors). The models used in the analysis are similar to those used in the analysis described above, i.e., a Gaussian size distribution of spherically symmetrical particles consisting of shells.

The fit to the data is presented in Fig. 7, and the radial density distributions for the average particle sizes are

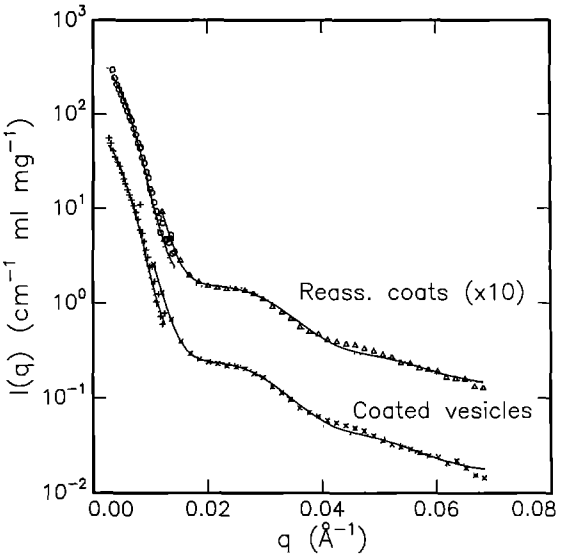

Fig. 6. Small-angle neutron scattering data for samples in 100% D_2O. *Upper data points:* reassembled coats. The data are multiplied by 10. *Lower data points:* native coated vesicles. The solid lines are the fits of the two-shell model, smeared by instrumental resolution. The dotted lines are the corresponding ideal fits. The statistical errors on the measured data are of the order of the size of the symbols

Table 3. Results for the neutron scattering data in 100% D_2O for coated vesicles and reassembled coats. The results are given for the particles of average size R_1

	Coat. vesic. 100% D_2O	Reass. coats 100% D_2O
Δr [Å]	175±5	157±5
R_1 [Å]	413±2.2	409±2.1
R_2 [Å]	184±1.7	182±0.6
R_3 [Å]	99±2.4	114±0.9
R_1-R_2 [Å]	229±2.8	227±2.2
R_2-R_3 [Å]	85±2.9	68±1.1
R_m [Å]	166±3	–
M [10^6 Da]	35.5±5	26.4±5
M_p [10^6 Da]	31.7	26.4
$M_{p,1}$ [10^6 Da]	23.1	15.3
$M_{p,2}$ [10^6 Da]	8.6	11.1
$M_{p,2}/M_p$	0.27	0.42
M_l [10^6 Da]	3.8	0

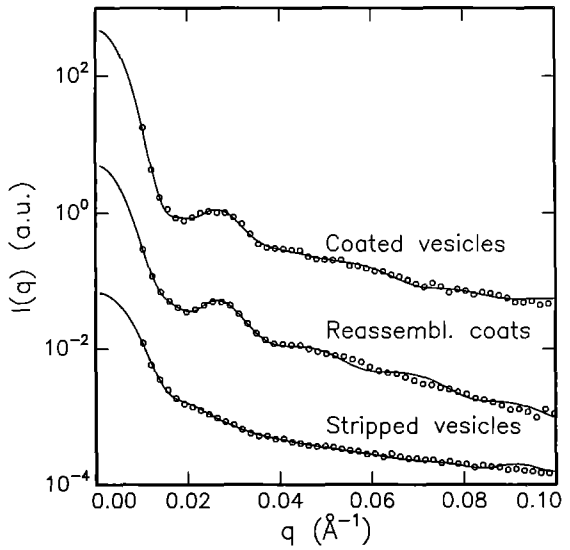

Fig. 7. Small-angle X-ray scattering data. *Upper data points:* native coated vesicles. *Middle data points:* reassembled coats. *Lower data points:* stripped vesicles. The curves are the fits of the best (higher resolution) models presented in the last part of Sect. 3. The corresponding radial density distributions for the average particle sizes are shown in Fig. 8

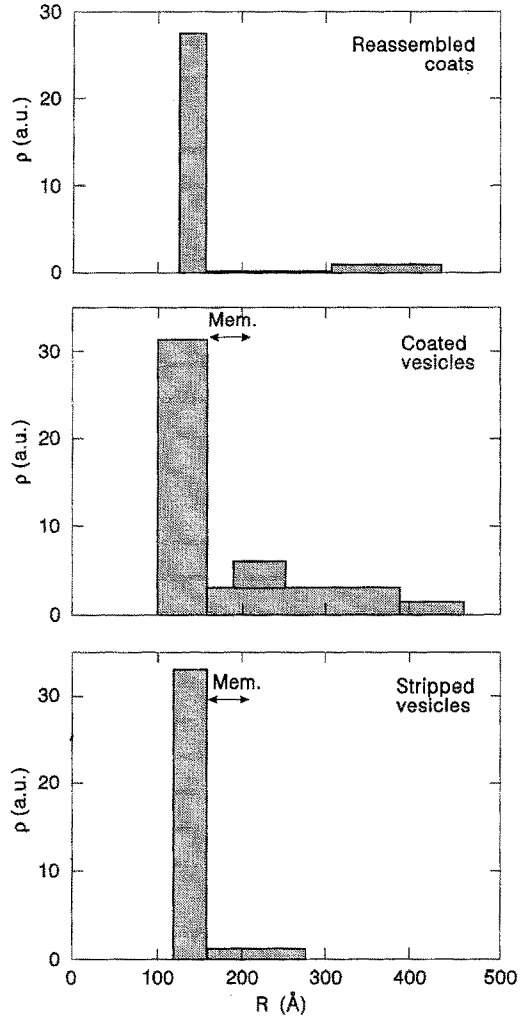

Fig. 8. Radial protein densities, from the X-ray scattering data, of the average particle for the best models. The densities correspond to the fits shown in Fig. 7

Table 4. Results from the X-ray data for the best (higher resolution) models. The radii are for the average particle. The densities are in arbitrary units and can only be compared within each column. The shell for the coated vesicles given by R_5 and R_6 is added to the shell and density given by R_2 and R_3 (see Fig. 8). The mass ratio M_2/M is the mass in the inner high density shell divided by the total mass

	Reass. coats	Coated vesic.	Stripped vesic.
Δr [Å]	77±2	72±1	127±3
R_1 [Å]	433±3	459±4	–
R_2 [Å]	304±5	390±3	277±7
R_3 [Å]	157±4	159±4	158±64
R_4 [Å]	127±4	97±5	121±4
R_5 [Å]	–	275±7	–
R_6 [Å]	–	191±32	–
ϱ_1 [a.u.]	2.85±0.1	1.4±0.1	–
ϱ_2 [a.u.]	1.1±0.2	3.2±0.1	1.1±0.1
ϱ_3 [a.u.]	84.6±21	32±2	34±5
ϱ_4 [a.u.]	–	2.6±0.7	–
M_2/M	0.47±0.1	0.28±005	–

shown in Fig. 8. We first note that for these models the values of the reduced χ^2 (see e.g. Bevington 1969) are about a factor of two to four smaller than for the lower resolution models. So from a statistical point of view it is justified to include the additional parameters in the model. The parameters for the best fits are displayed in Table 4. The polydispersity of the reassembled coats and the coated vesicles is similar (~75 Å), whereas that for the stripped vesicles is significantly larger (127 Å). The radial density distribution function for the reassembled coats (Fig. 8) displays a pronounced outer shell in the range 300 to 430 Å, which can be associated with the clathrin coat. The radial distribution of the coated vesicles is quite similar to the one found from the first two-shell model, with some additional density in the range 190 to 255 Å and in the range 390 to 460 Å. For the stripped vesicles, density is found outside the central main shell (120–160 Å) in the range up to 280 Å. The mass ratio M_2/M of the mass in the high-density shell to total mass is given in Table 4. For the coated vesicles only the mass for the radius <159 Å is included in M_2. This choice is somewhat arbitrary as one could argue that the range up to 255 Å should belong to the central part of the particle. This would give a much closer agreement with the mass ratios given in Table 1.

4. Discussion

Eight different X-ray and neutron scattering data sets have been analyzed by one common model. Polydispersity of the particles, in terms as a Gaussian distribution, is included in the model in such a way that the particles have a coat of constant thickness. The main features of the structure are a low-density outer protein shell of thickness 200–300 Å and a central high-density protein shell with a thickness less than 80 Å. In the analysis of neutron scattering from the coated vesicles, the presence of a lipid membrane shell of thickness 40 Å that overlaps

with the central protein shell was found. Owing to the low scattering contrast of X-rays for lipids, the membrane was not included in the model for the X-ray scattering data on coated and stripped vesicles. For the analysis of the data from stripped vesicles, the model was modified such that it did not include the outer protein shell.

In the appendix the possible systematic errors from neglecting the deviations from spherical symmetry in the model used in the data analysis is investigated in detail. The calculations lead to the conclusion that this neglect gives rise to an error on the structural parameters with an upper limit of about 10%, whereas the upper limit on the error on the molecular mass is about 20%.

The polydispersity for the experimental data varies a lot between different sample preparations. However, all values are much larger than the about 7% that might arise from the eccentricity of the particles (see the Appendix). The X-ray scattering (Bauer et al. 1991) from coated vesicles and reassembled coats show a polydispersity of about 80 Å (18%), whereas the stripped vesicles have a polydispersity of 130 Å. The neutron scattering from samples in 100% D_2O shows significantly larger polydispersity ($\sim$40%) than that from the corresponding X-ray scattering data. Even the data for the neutron contrast variation study exhibit a variation in polydispersity, despite the fact that the basic material of the samples was prepared in the same procedure. Fits to the individual contrasts give polydispersities of 18% for the D_2O sample, 27% for the 75% D_2O sample, and 31% (relative to an outer radius of 400 Å) for the 42% D_2O sample. The differences in the polydispersities of the neutron scattering samples are qualitatively confirmed by the dynamic light scattering measurements performed by Bauer et al. (1991, 1992). All of the samples were prepared from bovine brains, so there should be no difference in the original material. Also the sample preparation procedures used are nearly identical. Therefore, the conclusion that can be drawn is that the polydispersities of the samples are quite sensitive to minor changes in sample preparation procedure.

Comparison of the structural models

First, we will discuss the structure of the coated vesicles with reference to the structure (Fig. 5) determined from the neutron contrast variation data. This structure is based on three data sets measured at different contrasts, and it is therefore also the most reliable with respect to the identification of the protein and lipid contributions. Furthermore, the modest polydispersity for the three data sets should only cause small systematic errors. For this model, the outer radius of average particles is close to 400 Å, and the central high-density shell has outer and inner radii of 190 and 115 Å, respectively. We associate the outer shell with the clathrin protein and the inner shell with the accessory polypeptides and receptor proteins. We return to this point in the next section. The lipid membrane has an outer radius of 196 Å and a thickness of 40 Å. For the 100% D_2O data, a relatively large polydispersity is found, and, consequently, the structural parameters derived from this data are less reliable. However, the structure (Fig. 5) is quite similar to the one derived from the contrast variation data, except that the membrane has a 30 Å (15%) smaller radius. As mentioned previously, the identification of the lipid membrane is less reliable in this case, as it is only based on one contrast. The structure for the X-ray scattering data from the two-shell model (Fig. 3) has smaller radii for the average particle size. Adding 25 Å to the values brings the radius of the outer shell and the inner radius of the high-density shell into reasonable agreement with the neutron structures. However the outer radius of the high-density shell is some 30 Å lower than for the neutron models. This is probably due to the lipid membrane having a negative scattering density, which reduces the total scattering density in the region 150–190 Å. The position of the membrane is indicated in Fig. 3. For the best fit to the X-ray scattering data, the profile (Fig. 8) agrees well with the presence of a negative density membrane at 160–200 Å. The central protein has its major density inside the membrane, but also some density outside the membrane in the region 190–260 Å.

The one-shell model (Fig. 3) for the X-ray scattering data from the stripped vesicles has a shell thickness which is only slightly smaller than the thickness of the central shell in the two-shell model for the X-ray data for coated vesicles. It is therefore likely that the shell for the stripped vesicles corresponds to the protein, and that the membrane is in the region 150–190 Å and therefore almost enwraps the protein. The two-shell model (Fig. 8) for the stripped vesicles has additional density ranging up to 275 Å. This model is very similar to the best model for the coated vesicles for radii smaller than 275 Å. We conclude that the stripped vesicles contain a large portion of protein and receptors.

The two-shell model for the 100% D_2O neutron scattering data for the reassembled coats gives structural parameters (Table 3 and Fig. 5) which are nearly identical to those of the coated vesicles derived from the contrast variation and 100% D_2O neutron data. Comparing only the 100% D_2O results for the coated vesicles and reassembled coats (for data taken in the same run and with similar polydispersity) the main differences are a smaller thickness of the central high-density shell and a higher fraction of the protein in this shell for the reassembled coats. The differences are also found when comparing the results from the X-ray data for the two-shell model (Table 1) and for the best models (Table 4). However, the conclusions for the X-ray data are less firm owing to differences in the outer shell radius and the presence of the negative density membrane in the coated vesicles. The best model for the reassembled coats (Table 4 and Fig. 8) does not have a constant density in the outer low density region, but has an outer shell of thickness 130 Å with a higher density than in the intermediate region from 304 to 157 Å. This is probably due to the outer clathrins polygonal shell being resolved because of a relatively small polydispersity. Note that the density profiles, shown in Fig. 1, derived from cyro-electron microscopy (Vigers et al. 1986 b) display a similar shell structure. For the best model for the X-ray data on coated vesicles a similar shell structure is not found.

Composition and molecular mass

In the previously published analysis of the neutron contrast variation data (Bauer et al. 1992), the distance distribution functions were used for calculating the forward scattering. The variation of the forward scattering with D_2O percentage was used for determining the composition of the particles and the molecular mass. It was implicitly assumed that the samples were monodisperse. The analysis gave a composition of $25 \pm 5\%$ lipids and $75 \pm 5\%$ proteins, and a molecular mass of $(34 \pm 5) \times 10^6$ Da. The model fitting in the present work gives an average composition of 14% lipids and 86% protein. The discrepancy between these results is due to a different interpretation of the low-q part of the data. In the analysis of Bauer et al. the entire variation was assumed to be due to contrast variation, whereas in the model fitting here, some of the variation is neglected as being due to aggregation effects or differences in polydispersity. We believe that the values from the model fitting are more precise, as they are based on the consistency of the model with all three data sets. The molecular mass from the model fitting is determined to be $(27 \pm 4) \times 10^6$ Da from the contrast variation and $(36 \pm 5) \times 10^6$ Da for the 100% D_2O data. Note that the results in the appendix indicate a possible additional systematic error in these values of $\sim 10\%$. We consider the value for the 100% D_2O data to be the less accurate, as this sample has a very high degree of polydispersity. The difference in the molecular mass for the two ways of analyzing the contrast variation data is mainly due to the difference in the composition used in the two calculations. The molecular mass of the reassembled coats of $(26 \pm 4) \times 10^6$ Da determined from the 100% D_2O data is quite similar to the molecular mass of the coated vesicles.

The composition and molecular mass of the barrel structure can be estimated from the data compiled by Pearse and Crowther (1987) and the suggested packing of the clathrin in the coats (Crowther et al. 1976; Crowther and Pearse 1981). The best estimate of the radius of the barrel structure is probably from the cryo-electron microscopy investigations (Vigers et al. 1986 a, b), which suggest an average outer radius of 400 Å, taking the eccentricity of the barrel into account. The suggested packing (Crowther et al. 1976; Crowther and Pearse 1981) with one triskelion at each vertex, gives a total of 36 triskelions in the barrel. The triskelion consists of three heavy chain clathrin molecules of 180 kDa and three light chain clathrin molecules of approximately 35 kDa (Pearse and Crowther 1987), giving a total mass of 630 kDa. Thus, the clathrin in the barrel structure has an estimated molecular mass of 22.7×10^6 Da. The 20, 50, and 100 kDa accessory polypeptides forms aggregates consisting of one 20 kDa, one 50 kDa, and two 100 kDa polypeptides. This gives a total mass of about 300 kDa of the aggregate (see e.g. Heuser and Keen 1988; Pearse and Robinson 1990). The ratio of 100 kDa polypeptide to clathrin triskelion appears to be in the range 2–3 in reassembled coats (Pearse and Robinson 1984; Keen 1987). This gives a molecular mass of the accessory polypeptide in the reassembled coats in the range of 11×10^6 to 16×10^6 Da. The amount of accessory polypeptides seems to be smaller in coated vesicles. The work of Heuser and Keen (1988) suggests a mass of about 3×10^6 Da in coated vesicles with the barrel-shaped coating. From these values, the total mass of the reassembled coats is $34-39 \times 10^6$ Da, and the minimum protein mass in a coated vesicle is 26×10^6 Da for barrel-shaped structures. The accessory polypeptides constitute 32–41% of the mass of the reassembled coats and only 12% of the coated vesicle protein mass.

The value of the outer radius of the barrel structure, estimated from the cryo-electron microscopy results, is in excellent agreement with the value for the average particle found in the present work both for coated vesicles and reassembled coats. It has previously been claimed (Pearse and Crowther 1987) that the barrel-shaped structures do not contain vesicles. However, this was based on the assumption that the vesicles should be present inside the shell of accessory polypeptides. The present work shows that the accessory polypeptides are actually incorporated in the lipid membrane. In order to test the significance of this conclusion, a fit to the neutron contrast variation data was performed with a model that did not have vesicles in the smallest coats. The limit between coats with and without coats was described by a smooth function which allowed the parameter describing the limit to be fitted. In the optimization, the limit moved toward a small value (~ 140 Å) and had no significant influence on the model. Therefore, the neutron data does not support the suggestion that the barrel-shaped coats do not contain vesicles.

By assuming that the average particles have a barrel shape, one can compare the masses determined from the neutron scattering with those estimated above from other techniques by adding the molecular masses of the components (clathrin and accessory polypeptides). For the reassembled coats, the mass determined from the neutron scattering is smaller than the estimated value. The difference is about 25%, which is larger than the uncertainty on the experimentally determined mass, including a possible systematic error of about 5–10%. However, for the mass distribution between the central high-density shell, and the outer-low density shell the agreement is very good. The neutron scattering result that gives 42% of the mass in the central shell agrees with the estimate for 11×10^6 Da accessory polypeptides.

For the coated vesicles, there is nearly perfect agreement between the total protein mass determined from the neutron scattering and the estimated value. However, the mass distribution determined from the neutron scattering data does not agree with the expected mass distribution. The portion of the protein in the central shell is much higher in the neutron results. This is probably due to the presence of a significant amount of receptor molecules in the membrane. If we take this into account, the estimated value of the total protein mass is of the same magnitude as the mass of the reassembled coats. This suggests that for the coated vesicles there is also a disagreement between the total mass from the neutron scattering and the estimated value. It should be noted that the association of the average particle size with the barrel structure is connected with some uncertainty. We therefore only con-

clude that the average-size particles have masses which are about 25% smaller than those expected for barrel-shaped particles of coated vesicles and reassembled coats. However, we believe that the results gives strong support for the conclusion that the accessory polypeptides are situated in the lipid membrane in the native coated vesicles.

Densities and packing of components

For the neutron scattering data, the molecular masses of the various shells and components have been determined. By simply dividing the masses by the volume of the corresponding shells the densities can be calculated. These values can be compared to the densities derived from the specific volume and the expected hydration. For the proteins, the specific volume is about 0.75 cm^3/g (see Cusack et al. 1985) corresponding to a density of 1.33 g/cm^3. For close packing of globular, spherical-shaped proteins, a good estimate of the volume fraction is 0.7, giving a hydrated density of ~ 1.0 g/cm^3. This value agrees with the density in the protein capsid of many simple vira (Chauvin et al. 1978, 1979; Cuillel et al. 1981; Devaux et al. 1983; Berthet-Colominas et al. 1986). The lipids have a specific volume of 0.96 cm^3/g, corresponding to a density of 1.04 g/cm^3 (Cusack et al. 1985). Allowing the lipids to have a non-dense packing reduces the density to 0.8–0.9 g/cm^3 for 10–20% free space in the lipid bilayer. This density is similar to the one for the membrane in influenza virus (Cusack et al. 1985), which also contain small amounts of trans-membrane glyco-proteins.

The model for the coated vesicles derived from the contrast variation data has three components: An outer protein shell, an inner protein shell and a lipid membrane. The outer protein shell has a density of $\varrho_{p,1} = 0.10$ g/cm^3. As already mentioned, we associate the outer protein shell with the clathrin polygonal lattice and the low density in the outer shell is obviously connected with the open structure of the lattice. The inner shell has a density of $\varrho_{p,2} = 0.66$ g/cm^3. The membrane shell, which overlaps with the inner protein shell has a density of $\varrho_m = 0.41$ g/cm^3. From these two values, one sees that the hydration is very low in the region with the membrane. The corresponding densities for the model for the 100% D_2O data are: $\varrho_{p,1} = 0.14$ g/cm^3, $\varrho_{p,2} = 0.65$ g/cm^3 and $\varrho_m = 0.59$ g/cm^3. These values agree reasonably with those for the contrast variation structure. The differences might be due to the larger uncertainties in the parameters in the fit of the model for the 100% D_2O data, owing to the larger polydispersity of this sample.

For the reassembled coats, the density of the outer shell is $\varrho_{p,1} = 0.10$ g/cm^3 and the density of the inner shell is $\varrho_{p,2} = 1.0$ g/cm^3. The value of $\varrho_{p,1}$ is identical to the value for the structure of the coated vesicles derived from the contrast variation series. The density $\varrho_{p,2}$ of the inner shell is higher than that for the coated vesicles. The value is close to those found for the protein capsids of virus particles, and it shows that the hydration of the layer is very small.

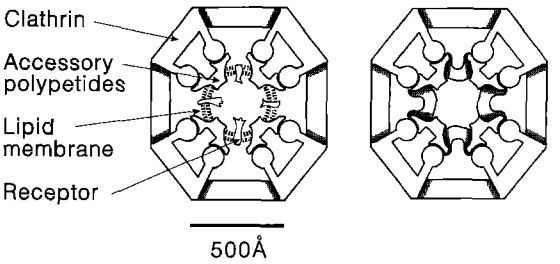

Fig. 9. Schematic drawings of the coated vesicles (*left-hand side*) and reassembled coats (*right-hand side*). Cuts through the center of barrel-shaped particles are shown

5. Summary and conclusions

The analysis of the small-angle scattering data has shown that the structures of the coated vesicles and the reassembled coats are very similar. The main new conclusions from the present work are: (*i*) The smaller particles from preparations of coated vesicles also contain a lipid membrane. (*ii*) The position of the membrane coincides with the central high-density protein shell, and consequently, the membrane contains a large amount of protein. (*iii*) The structures of the native coats and the reassembled coats are very similar.

The discussion of the densities of the central shell demonstrates a nearly constant density of material in the central high-density shell of the particles. For the coated vesicles, protein and membrane both contribute to the density, whereas for the reassembled coats, the membrane contribution is 'replaced' by additional protein. This leads us to suggest the schematic models shown in Fig. 9, which also incorporate some of the structural information from cryo-electron microscopy (Vigers et al. 1986 a, b). The structures are shown as cuts through the center of barrel-shaped particles. For the coated vesicles, the results that the accessory polypeptides are situated in the cell membrane. These molecules probably work as receptors for the clathrin molecules when the clathrin lattice is formed. When reassembling the purified components of the coats, the hydrophobic parts of the accessory polypeptides combine and the polypeptides form a dense shell. The clathrin lattice is then formed around this shell by connecting to the receptor-like parts of the accessory proteins.

We will finally summarize in greater detail the justifications for the models shown in Fig. 9. For the reassembled coats the X-ray and neutron scattering density distributions give a total coat thickness of 300–330 Å, in close agreement with the cryo-electron microscopy results of Vigers et al. (1986 b) (see also Fig. 1). If the average-size particle is associated with the barrel structure, which has nearly the same size, one sees from the Figs. 1, 3, 5, and 8, that the mass distribution determined from the scattering experiments is quite different from the one determined by electron microscopy (Vigers et al. 1986 b). The scattering experiments give a much higher density in the central shell than in the outer shell, whereas electron microscopy gives a more homogeneous density. The total mass and the mass distribution deduced from the neutron experiments in 100% D_2O, and the expected ratio of clathrin to

accessory polypeptides (Pearse and Robinson 1984; Keen 1987; Ahle et al. 1988) suggest that the central shell consists of accessory polypeptides (and receptors) and that the outer shell consists of clathrin.

For the native coated vesicles both the electron microscopy (Vigers et al. 1986 b) and the scattering experiments give a total coat thickness of 300–320 Å in close agreement with the results for the reassembled coats. Also the distribution of the protein with a high density central shell is quite similar for the electron microscopy and the scattering experiments. If the average-size particle is again associated with the barrel structure the mass and the mass distribution determined from the neutron scattering data strongly indicates that the low-density outer shell is due to clathrin and that the high-density central shell consists of accessory polypeptides and receptors. This interpretation is quite different from the one by Vigers et al. (1986 b). They interpreted the low-density shell to be due to clathrin and accessory polypeptides, and the high-density shell to be due to other proteins situated in the membrane. With their interpretation the coat thickness (clathrin and accessory polypeptides) is about 40 Å smaller than for the reassembled coats.

With the assignment of the central shell to the accessory polypeptides and receptors, the position of the membrane determined by the neutron scattering experiments is within this shell. This is in contrast to the previous suggestion (Vigers et al. 1986 b; Pearse and Crowther 1987; Pearse and Robinson 1990) that the accessory polypeptide are outside the membrane and connected to the cytoplasmic part of the receptors. We have found that it is not possible to fit the neutron contrast variation data with the membrane at significantly smaller radius. We therefore believe that the results strongly support the model for the coated vesicles shown in Fig. 9. The position of the membrane is further supported by the X-ray scattering results (Figs. 3 and 8), which shows a narrower central shell and a total coat thickness similar to the one determined from the neutron scattering data. As the lipid membrane is expected to have a negative scattering density for X-rays the position is likely to be close to the outside of the high-density shell.

The position of the accessory polypeptides within the lipid membrane is, however, surprising as the accessory polypeptide complexes are not know to be integral membrane proteins. This point should be investigated further in the future.

Acknowledgements. The work was supported by the Danish Natural Science Council. Numerous fruitful and illuminating discussions with Kell Mortensen and Steen Hansen are gratefully acknowledged. The collaboration with Gareth Jones, Moira Behan, and David Clark during the work described in Bauer et al. (1992) is also gratefully acknowledged. Finally, I wish to thank David Pengra for his comments on the manuscript and correction to the English.

Appendix: Deviation from spherical symmetry

In this appendix, the possible influence on the results of deviation from spherical symmetry of the particles is investigated. It is well known that the finer details of a structure can have a pronounced influence on the corresponding small-angle scattering curve (Jack and Harrison 1975). For example, for scattering from icosahedral capsids consisting of globular protein, the packing arrangement gives rise to large broad bumps at intermediate values of the scattering vectors (Chauvin et al. 1978; Cusack et al. 1981). The position of the bump is related to the characteristic distance d between the proteins as $q \sim 2\pi/d$. For the clathrin coats, numerous electron microscopy studies have shown a characteristic arrangement of the clathrin, which consists of a polygonal network of hexagons and pentagons (Pearse and Crowther 1987, and references therein). In the following, scattering curves from models containing these features are generated, and subsequently analyzed by spherical models in order to determine the systematic errors in the structural parameters arising from these features.

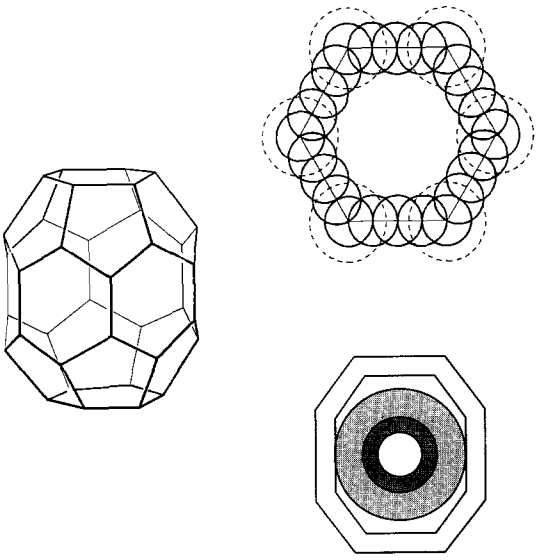

Fig. 10. The structure used in the model calculations. The left-hand side shows the barrel composed of hexagons and pentagons. The right-hand side shows the positions of the spheres, making up the coat structure. The circle shown by a broken line indicates the positions of the sphere in model (II), which simulates the extra mass below the coat. Also shown is a cut through the center of the structure, showing the central shells

Several structures have been found experimentally (Crowther et al. 1976), and among these is the barrel-shaped one, which is shown in Fig. 10. It would be an overwhelming job to calculate the scattering of all the different structures and we have therefore restricted our investigation to the barrel structure. This structure is also the most frequent one observed for reassembled coats (Pearse and Robinson 1984). The coat of barrel-shaped particles has two contributions to the deviation from spherical symmetry: First, the already mentioned polygonal net in the surface; second, the eccentricity of the barrel, which is similar to a prolate ellipse. The barrel structure is probably the particle with the largest eccentricity. Both the smaller and larger coats have shapes that are more spherical (Crowther et al. 1976). The small-angle scattering curves of the model structures were calculated by means of the well-known Debye formula as described

by Glatter (1972). For spherically symmetrical sub-units, the scattering from an assembly of randomly oriented particles is given by:

$$\frac{d\sigma(q)}{d\Omega} = \sum_{i=1}^{N} \sum_{j=1}^{N} \varrho_i \Phi_i(q)\, \varrho_j \Phi_j(q) \frac{\sin(q\, d_{ij})}{q\, d_{ij}} \qquad (13)$$

where ϱ_i is the scattering density of the ith sub-unit, which has the form factor $\Phi_i(q)$, given by an expression similar to Eq. (6). The parameter d_{ij} is the distance between the ith and the jth sub-unit, and N is the number of sub-units.

First, the scattering curve from an empty shell is calulated. The barrel structure (Fig. 10) has one hexagon at the top and one at the bottom, and it has further a ring of six hexagons around the 'belly'. Two rings each of six pentagons connect the top and bottom hexagons to the ring around the 'belly'. In the model, all the sides in the pentagons and hexagons are taken to have the same length, and this gives an eccentricity of about 1.2. A total of 198 spheres is placed along the sides, as indicated on the figure. The dimensions of the barrel are estimated from the electron micrographs of Vigers et al. (1985 a, b). The distance from the center of the barrel to the vertices closest to the 'belly' is 350 Å, and the radius of the spheres is 50 Å. The vertex-vertex distance is 194 Å, and with a distance of 49 Å between the centers of the spheres, there is no significant influence of the regular spacing of the spheres for $q < 0.1$ Å^{-1}. When calculating the scattering curves, the full (622) symmetry of the barrel is used in order to reduce the number of terms that have to be calculated in (13). For all the calculated model scattering curves, 3% relative Gaussian distributed noise is added in order to allow analysis of the curves by the least-quares fitting routines used for the analysis of the experimental data. The calculated scattering curve for the barrel is shown in Fig. 11 as 'experimental' points. The curve has a pronounced minimum at $q = 0.09$ Å^{-1} owing to the form factor of the thickness of the coating shell. When fitting a model of a spherical shell to the generated scattering curve, the thickness of the shell has to be fixed at 70 Å in order to reproduce the minimum. The outer radius of the shell was determined to be 417 Å by fitting the low-q part of the data ($q < 0.01$ Å^{-1}). The fit is shown as the solid line in Fig. 11. Owing to the spherical symmetry, the minima and maxima are much more pronounced than in the simulated curve. There are also significant deviations in the range $q > 0.02$ Å^{-1} due to the internal structure of the shell. Introducing a polydispersity of 30 Å in the fitted models in terms of a Gaussian distribution gives a smearing of the maxima and minima which is somewhat smaller than the smearing in the simulated curve. However, the minimum at 0.09 Å^{-1} originating from the coat thickness is, with this polydispersity, more smeared than in the simulated data. The simulated scattering data have a significantly higher intensity for $q > 0.02$ Å^{-1} than the curve given by the spherical model. Note that the integrated scattering (volume times scattering density) of the two curves are identical. A fit of an elliptical shell to the data does not give better agreement with the maxima and minima in the simulated data. This is due to the smearing mainly being caused by the internal structure of the shell, i.e. the pentagons and hexagons.

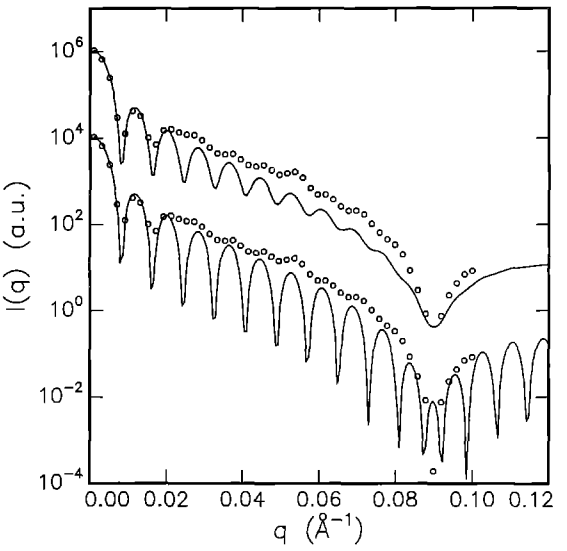

Fig. 11. Small-angle scattering from the an empty hexagonal barrel. The points are from the simulation and the curve is a fit of a model consisting of a thin shell. *Lower curve*: Fit of a monodisperse model. *Upper curve*: Fit of a polydisperse model. The upper scattering curves have been multiplied by 100

In the following, the scattering curves of two structures, similar to those determined from the experimental data, are investigated for different polydispersities. In the models, a Gaussian polydispersity similar to the one described in Sec. (2) is used. The thicknesses of the various shells are kept constant. Introducing polydispersity of the radii of the shells in the barrel structure is of course, not the most realistic approach, as this would make the side length of the polygons in the structure change. This length is likely to be constant, and the difference between particles of different size is the number of hexagons they have. However, the features in the scattering curve originating from the internal structure of the coats are very broad, and, therefore, a polydispersity of a reasonable magnitude is mainly smearing the maxima and minima in the scattering curves with a modest influence on the other features. In order to avoid a lower density in the coat when rescaling the radius of the shell, the radius of the spheres are scaled with the factor $(R_1 + r)/R_1$, where R_1 is the radius of the outer shell for the average particle and r is the deviation in size. We note that in the actually measured samples the eccentricity of the particles is in general smaller than for the model as most of the structures have nearly spherical shapes. Therefore the influence of eccentricity is larger when analyzing the simulated data than when analyzing the experimental data.

The two models that have been used both have a central spherical shell of high scattering density with an inner radius of 115 Å and an outer radius of 190 Å. Model (I) has a spherical shell of low density with an inner radius of 190 Å and an outer radius of 340 Å. This shell corresponds to the terminal domains of the clathrin triskelion, which connects the outer polygonal coat to the inner protein shell. It is also possible that this shell includes the light chains, which are known to be situated near the center of the triskelions (Ungewickell 1983; Kirchhausen et al. 1983). Setting the total scattering length (scattering-

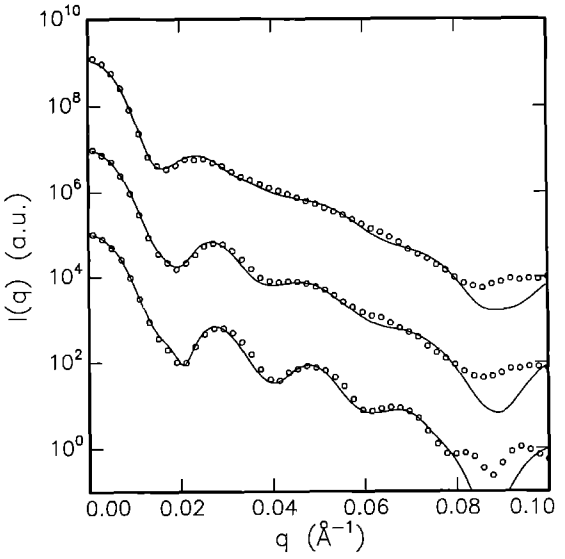

Fig. 12. Small-angle scattering from the model (I). The points are simulated data for polydispersities 100, 40, and 15 Å, going from top to bottom. The two upper curves have been multiplied by 100 and 10,000, respectively. The full curves are fits of the polydisperse two-shell model

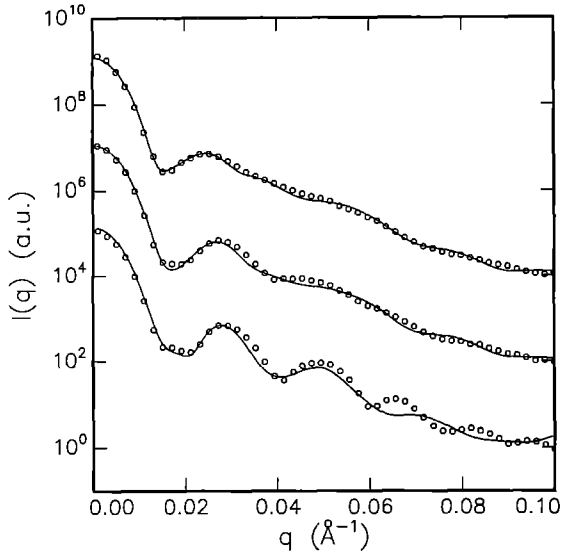

Fig. 13. Small-angle scattering from the model (II). See the legend of Fig. 12 for additional information

length density times volume) of the outer barrel equal to unity, the scattering length of the middle shell is 0.769 and the scattering length of the central shell is 1.267. Assuming that the particles contain only one kind of material (i.e., protein), this corresponds to a mass fraction of 0.42 for the inner shell, in accordance with the mass fraction for the experimental data.

In the model (II), the middle shell is replaced by 36 spheres of radius 75 Å which are placed under the vertices of the polygonal network of the coat. This is in agreement with the cyro-electron micrographs (Vigers et al. 1985 b), which reveal protein at these positions. The distance from the center of the barrel to the spheres closest to the 'belly' is 275 Å. The total scattering length of outer shell and the central shell are the same as for model (I), and the total scattering length of the 36 spheres in the intermediate region is equal to unity. This gives as mass fraction of 0.39 of the inner shell for this model.

The scattering curves of the two models are shown in Figs. 12 and 13 for polydispersities of 15, 40, and 100 Å, corresponding to 3.6, 9.6, and 24% polydispersity, relative to an outer radius of 417 Å. The curves for the two models are surprisingly similar, considering that model (II) has a much larger fraction of material arranged in accordance with the symmetry of the barrel. The fraction is 0.60 as compared to 0.33 for model (I).

The simulated scattering data are analyzed similarly to the experimental data using least-squares optimization of a polydisperse two-shell model. The results are given in Table 5, together with the parameters of the original models (in the parenthesis). All the values given in the table are for the particles with average size. The results for the two models are very similar, and the parameters agree quite well with the original values. The largest discrepancies are for the determined polydispersities of the models with an original polydispersity of 15 Å. The values deviate by more than a factor of two from the original one. This is probably due to the eccentricity of the particles, which smears out the features in the scattering curve. By comparing with the results for the empty barrel, it seems reasonable to conclude that the eccentricity gives rise to an effect which is similar to a polydispersity of about 30 Å. For the models with an original polydispersity of 100 Å, the values are underestimated by 40% for model (I) and

Table 5. Results of the analysis of the simulated scattering curves in Figs. 12 and 13 for the models (I) and (II) described in the text. The model used in the least-squares analysis is a polydisperse two-shell model. The radii and masses are for the average particle. The masses are in units of the mass of the outer polygonal coat. The numbers in parenthesis are the values of the parameters for the original models. When only given in the first column, the values are the same for the whole row

	Model (I)			Model (II)		
Δr [Å]	31 (15)	50 (40)	80 (100)	42 (15)	56 (40)	66 (100)
R_1 [Å]	443 (417)	438	449	428	423	432
R_2 [Å]	189 (190)	192	210	188	195	213
R_3 [Å]	116 (115)	119	137	113	127	144
$R_1 - R_2$ [Å]	254 (227)	246	239	240	228	219
$R_2 - R_3$ [Å]	73 (75)	73	73	75	68	69
M_1/M	0.57 (0.58)	0.54 (0.58)	0.47 (0.58)	0.62 (0.61)	0.55 (0.61)	0.61 (0.49)
M_2/M	0.43 (0.42)	0.46 (0.42)	0.53 (0.42)	0.38 (0.39)	0.45 (0.39)	0.51 (0.39)
M [a.u.]	1.02 (1.0)	0.95	0.94	1.16	0 93	0.96

33% for model (II). The values for the radii agree within 10% with the original values, for the models with original polydispersities of 15 and 40 Å. Note that for all models, the thickness of the shells are reproduced with less than 10% deviations. For the models with 100 Å polydispersity, all the radii are overestimated by 10–15%. The large particles dominate the scattering curve, owing to the weighting according to the square of the total scattering length (equal to the square of the mass for particles containing only one kind of material). A comparison of the average scattering weighted particles would give a better agreement. Note that these results demonstrate a low sensitivity to the small-size part of the size distribution. The discrepancies in the mass distribution found for the 100 Å polydisperse models are also mainly due to this effect. For the larger particles, a larger part of the mass is situated in the central high-density shell. The total mass M of the average particle is calculated as described in Sec. (4 b). The masses given in Table 5 are normalized so that the average particle has a mass of unity in the original models. Except for one calculation, the masses agree within 10% with the original ones.

The overall conclusion from the investigations described in this appendix is that the contribution from non-spherical effects has only a minor influence on the parameters determined by the least-squares analysis. The model with spherical symmetry can therefore be applied to the analysis of the experimental data. The systematic errors caused by the spherical approximation are, in most cases, about 10%. A large polydispersity might also cause systematic errors.

References

Ahle S, Ungewickell E (1986) Purification and properties of a new clathrin assembly protein. EMBO J 5:3143–3149

Ahle S, Mann A, Eichelsbacher U, Ungewickell E (1988) Structural relationships between clathrin assembly proteins from the Golgi and plasma membrane. EMBO J 7:919–929

Bauer R, Behan M, Hansen S, Jones G, Mortensen K, Særmark T, Øgendal L (1991) Small-angle scattering studies on clathrin-coated vesicles. J Appl Crystallogr 24:815–821

Bauer R, Behan M, Clark D, Hansen S, Jones G, Mortensen K, Pedersen J Skov (1992) Contrast variation studies of clathrin coated vesicles by small-angle neutron scattering. Eur Biophys J 21:129–136

Berthet-Colominas C, Boulanger P, Devaux C, Jacrot B, Timmins PA (1986) Structural studies of adenovirus type 2 and an assembly mutant. Biophys J 49:21–22

Bevington PR (1969) Data reduction and error analysis for the physical sciences. McGraw-Hill, New York

Bretscher MS, Thomson JN, Pearse BMF (1980) Coated pits act as molecular filters. Proc Natl Acad Sci, USA 77:4156–4159

Chauvin C, Witz J, Jacrot B (1978) Structure of the tomato bushy stunt virus: a model for protein-RNA interaction. J Mol Biol 124:641–651

Chauvin C, Jacrot B, Lebeurier G, Hirth L (1979) Structure of the cauliflower mosaic virus: a neutron diffraction study. Virology 96:640–641

Crowther RA, Pearse BMF (1981) Assembly and packing of clathrin into coats. J Cell Biol 91:790–797

Crowther RA, Finch JT, Pearse BMF (1976) On the structure of coated vesicles. J Mol Biol 103:785–798

Cuillel M, Jacrot B, Zulauf M (1981) A T=1 capsid formed by protein of brome mosaic virus in the presence of trypsin. Virology 110:63–72

Cusack S, Miller A, Krijgsman PCJ, Mellema JE (1981) An investigation of the structure of alfalfa mosaic virus by small-angle neutron scattering. J Mol Biol 145:525–543

Cusack S, Ruigrok RWH, Krygsman PCJ, Mellema JE (1985) Structure and composition of influenze virus. A small-angle neutron scattering study. J Mol Biol 186:565–582

Devaux C, Timmins PA, Berthet-Colominas C (1983) Structural studies of adenovirus type 3 by neutron and X-ray scattering. J Mol Biol 167:119–132

Glatter O (1972) X-ray small-angle scattering of molecules composed of subunits. Acta Phys Austriaca 36:307–315

Harrison SC, David A, Jumblatt J, Darnell JE (1971) Lipid and protein organization in sindbis virus. J Mol Biol 60:523–528

Heuser JE, Keen J (1988) Deep-etch visualization of proteins involved in clathrin assembly. J Cell Biol 107:877–886

Jack A, Harrison SC (1975) On the interpretation of small-angle X-ray solution scattering from spherical viruses. J Mol Biol 99:15–25

Jacrot B (1976) The study of biological structures by neutron scattering from solution. Rep Prog Phys 39:911–953

Keen JH (1987) Clathrin assembly proteins: affinity and a model for coat assembly. J Cell Biol 105:1989–1998

Kirchhausen T, Harrison SC, Parham P, Brodsky FM (1983) Location and distribution of the light chains in clathrin trimers. Proc Natl Acad Sci, USA 80:2481–2485

Marsh M, Helenius A (1980) Adsorptive endocytosis of semliki forest virus. J Mol Biol 142:439–454

Marquardt DW (1963) An algorithm for least-squares estimation of nonlinear parameters. J Soc Indust Appl Math 11:431–441

Pearse BMF (1975) Coated vesicles from pig brain: purification and biochemical characterization. J Mol Biol 97:93–98

Pearse BMF (1985) Assembly of the mannose-6-phosphate receptor into reconstituted clathrin coats. EMBO J 4:2457–2460

Pearse BMF, Robinson MS (1984) Purification and properties of 100-kd proteins from coated vesicles and their reconstitution with clathrin. EMBO J 3:1951–1957

Pearse BMF, Crowther RA (1987) Structure and assembly of coated vesicles. Ann Rev Biophys Chem 16:49–68

Pearse BMF, Robinson MS (1990) Clathrin, adaptors, and sorting. Ann Rev Cell Biol 6:151–171

Pedersen J Skov, Riekel C (1991) Resolution function and flux at the sample for small-angle X-ray scattering calculated in position-angle-wavelength space. J Appl Crystallogr 24:893–909

Pedersen J Skov, Posselt D, Mortensen K (1990) Analytical treatment of the resolution function for small-angle scattering. J Appl Crystallogr 23:321–333

Perkins SJ (1988) Structural studies of proteins by high-flux X-ray and neutron solution scattering. Biochem J 254:313–327

Perry MM, Gilbert AB (1979) Yolk transport in the ovarian follicle of the hen (*Gallus Domesticus*): Lipoprotein-like particles at the periphery of the oocyte in the rapid growth phase. J Cell Biol 39:257–272

Roman LM, Garoff H (1985) Revelation through exploration: the viral model for intracellular traffic. Trends Biochem Sci 10:428–432

Ruigrok RWH, Andree PJ, Hooft van Huysduynen RAM, Mellema JE (1984 a) Characterization of three highly purified influenza strains by electron microscopy. J Gen Virol 65:799–802

Ruigrok RWH, Nermut MV, Andree PJ (1984 b) The molecular mass of adenovirus type 5 as determined by means of scanning electron microscopy (STEM). J Virol Methods 9:66–78

Schneider D, Zulauf M, Schäfer R, Franklin RM (1978) Structure and synthesis of a lipid-containing bacteriophage. J Mol Biol 124:97–122

Sjöberg B (1978) A general weighted least-squares method for the evaluation of small-angle X-ray data without desmearing. J Appl Crystallogr 11:73–79

Unanue ER, Ungewickell E, Branton D (1981) The binding of clathrin triskelion to membranes from coated vesicles. Cell 26: 439–446

Ungewickell E (1983) Biochemical and immunological studies on clathrin light chains and their binding sites on clathrin triskelions. EMBO J 2:1401–1408

Ungewickell E, Branton D (1981) Assembly units of clathrin coats. Nature 289:420–422

Vigers GPA, Crowther RA, Pearse BMF (1986 a) Three-dimensional structure of clathrin cages in ice. EMBO J 5: 529–634

Vigers GPA, Crowther RA, Pearse BMF (1986 b) Location of the 100 kd–50 kd accessory proteins in clathrin coats. EMBO J 5: 2079–2085

Zaremba S, Keen JH (1983) Assembly polypeptide from coated vesicles mediate reassembly of unique clathrin coats. J Cell Biol 97:1339–1347